www.cadanda.com
Computer-Aided Design AND APPLICATIONS

Automatic Generation of Supported-postures using Digital Human Model

K.Eazhil Selvan[1], Dibakar Sen[1]

[1]Indian Institute of Science, eazhilsl@gmail.com,sendibakar1@gmail.com

Corresponding author: Dibakar Sen, sendibakar1@gmail.com

Abstract. Support taking through bracing or leaning while performing manual tasks is known to enhance the capability of the operator. However, simulation of this natural and biomechanically significant behaviour in a DHM environment is either not possible or calls for significant expertise and planning on the part of the simulation engineer. While manual simulation is time-consuming and error-prone, an algorithmic procedure is expected to enhance efficiency and versatility in the simulation of diverse work environments and what-if scenarios. This paper presents a computational method for determining the location of and reaction at a support point on a given surface that is most advantageous for performing a task. The method also evaluates different possible support combinations and the associated optimal postures for performing a given task. The method is illustrated through one-handed reach and supported sitting tasks. Given the task and the environment, the simulation is performed without the need for any user intervention.

Keywords: Digital Human Model; Supported-postures; Posture-prediction; Workspace-design; Computer Aided Design
DOI: https://doi.org/10.14733/cadaps.2023.382-401

1 INTRODUCTION

Resting different parts of the body while performing an activity is a common and natural human tendency. A survey [12] on tasks performed at an automotive factory reported that 48% of 910 incidences involved external support-taking. Another study [3] observed 250 tasks and found that 41.3% of the jobs involved leaning or bracing on objects available in the task environment.

It is observed in [6] and [16] that, through leaning or bracing, the maximum reach of the hand is increased by counteracting the destabilising moment incurred during extreme reach efforts. [17] observed that allowing bracing during force exertion task improved the force exertion capability. Later, [13] also showed that the presence of bracing surfaces at the hand and thigh increased the average force exertion capability of the task hand by up to 43%. [5] and [14] showed that taking support reduced spinal-loading for one-handed lifting tasks.

There are multiple challenges in the simulation of supported behaviour, viz. figuring out when is support taken and when not; which surface and where on it meaningful supports can be obtained and estimating the support reaction force (SRF) and their effect on the posture. The problem of estimating the supported-postures and the reaction forces using DHMs has been studied by [4],[10], [9]. The work by [4] is based on choosing a supported posture and then trying out different SRFs at support-contact to arrive at an acceptable force. The works by [10] and [9] describe the technique of computing supported-posture along with SRFs by considering the SRF as an optimisation variable when the location of support-contact is given. [2],[6] and [16] performed empirical studies and developed regression models to predict when and how the human will take support for a given task and anthropometry. Since the regression model is built on a selected set of tasks and environments, it may not be applicable for alternate scenarios. Therefore, a computational model based on a theoretical understanding of support-taking behaviour is necessary. No works on DHM-based computational models for the support-taking behaviour could be found in the literature by the authors.

In the conventional DHM systems, the designer is required to guess if support-taking is necessary for a task, as well as specify the location of the support for posture-prediction. The aim of the current work is to develop a computational framework that can automatically generate feasible supported postures for performing a task, using only the description of the task and the environment as input. Thus, for a given task description and the geometry of the environment, the system should assess if support taking is required and automatically identify suitable supports for executing the task. When supports are available, the system should generate multiple feasible supported postures using those supports. If support taking is required and no supports could be identified either because of the absence of supporting structures or the complexity of the geometry, the system should report that there are no feasible postures to execute the task.

2 POSTURE-PREDICTION

In this work, we are interested in computing static postures for simple reach or exertion tasks. For a simple reach, there is no load acting on the end-effector, while for exertion, forces and moments are applied at the end-effector. Now, given the task-specification and the support-surfaces, the supported posture for performing the task must be computed. This is done by optimising the posture to satisfy the constraints such as contacts, stability and joint-strength limitations. For a given support-surface, the exact point on the surface for making contact is an unknown variable. Since the system is statically indeterminate, the SRFs must also be computed. Therefore, while computing the joint-angle values, we also include the contact-locations and the SRFs by modelling them as optimisation variables.

2.1 Description of Digital Human Model

A DHM developed in-house by the authors has been used in this work. The DHM is modelled as an articulated tree structure made of rigid links or segments connected by joints, as shown in Figure 1. It is composed of 18 segments and has 41 degrees of freedom (DOF). The joints are modelled as spherical pairs using Euler angles; For revolute joints, only one of the three DOFs is used in the computation. The range of motion (ROM) is defined for each DOF. For each segment, the mass is assigned using the weight-proportion of the segment to the whole body's weight. The data for the ROMs of the joints and the weight-proportions of the segments were adopted from [1] and [18], respectively. The skeleton of each segment is represented using a line segment, and the skin is represented using a mesh, as shown in Figure 1a. The Centre of Mass (COM) location for each segment is defined at the centroid of the segment's skeletal geometry.

The anthropometry of the human can be modified by supplying the data on the length and width of the segments. For setting the anthropometry of the DHM to represent a real human subject, the subject is motion-captured, and a set of points that correspond to the relative positions of the joint-centres is obtained. The motion-capture system used in the current work represents each body-segment as a rigid body and outputs its

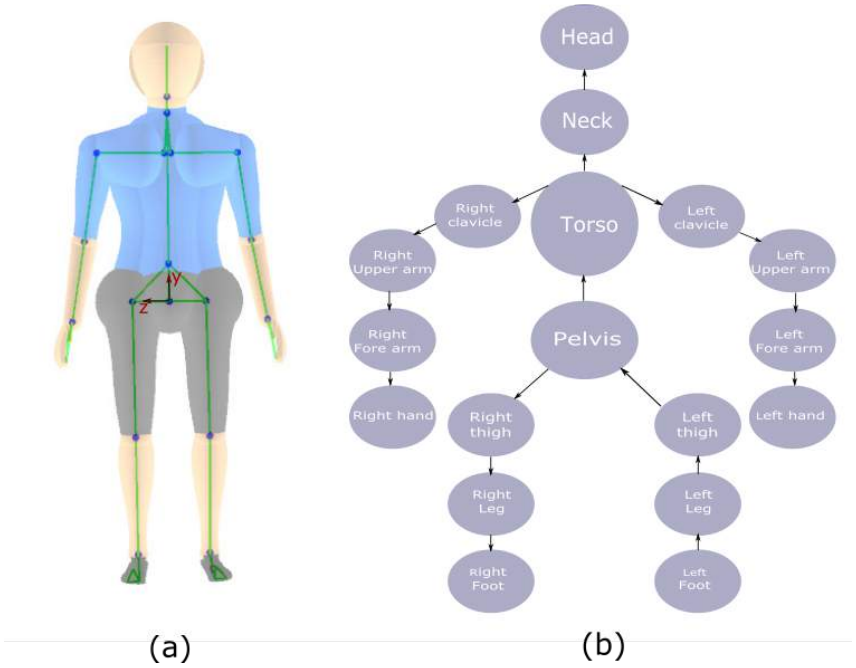

Figure 1: Digital Human Model: (a) Human-figure with skeletal structure. The local frame of reference is shown on pelvis (b)Tree representation of Kinematic-structure rooted at the left foot

configuration (position and quaternion) at different time stamps. Here, the origin of the frame of reference of the segment corresponds to the centre of the joint that drives that segment. Based on the distance between the joints, the segment lengths are obtained, and the DHM is scaled to match the human subject.

A local frame of reference $\mathcal{L}$ is defined for the DHM. The origin of the frame $\mathcal{L}_o$ is placed at the centre of the pelvis. At the standard anatomical position, the xy plane defines the sagittal plane, with the positive x-axis ($\mathcal{L}_x$) and y-axis ($\mathcal{L}_y$) pointing towards anterior and superior directions, respectively.

One speciality of the kinematic structure is that it is support-mutable, meaning any link of the tree-structure can be set as the root. Using the Euler angles for representing joints instead of the Denavit-Hartenberg convention makes it easier to represent a kinematic structure where the parent-child relationship between segments can be inverted. The freedom to choose the root of the tree is convenient since the main load-bearing segment of the body can be set as the root. However, there can be more than one supporting segment that can share the weight. Therefore, the segment corresponding to the root of the tree is called the primary support and the other supports are called auxiliary supports. For example, while standing on two legs, the foot corresponding to the root shall be called the primary support, while the other foot will be the auxiliary support.

2.2 Modeling Contact

A kinematic or reach goal requires the end-effector to be positioned and oriented in space as specified by a reach target. A configuration can be defined using three vectors: one vector for position and two orthogonal unit vectors for orientation. We use coordinate frames to represent the configurations and refer to them as *contact-sites*. Contact-sites are defined on both end-effectors and targets to represent their configurations. Let $\mathcal{E}$ and $\mathcal{T}$ denote the contact-sites corresponding to end-effector and target, respectively. For a given

frame, say $\mathcal{T}$, the position is represented by the origin of the frame $\mathcal{T}^o$ and orientations are specified by two of its axes $\mathcal{T}^x, \mathcal{T}^y$. The kinematic goal is said to be achieved when the positions of the frames are coincident ($\mathcal{E}^o = \mathcal{T}^o$) and two of the axes are facing each other ($\mathcal{E}^z = -\mathcal{T}^z$ and $\mathcal{E}^x = -\mathcal{T}^x$). The list of contacts to be achieved can be represented by the contact set C of pairs of end-effector and target-sites as, $C = \{(\mathcal{E}_1, \mathcal{T}_1), (\mathcal{E}_2, \mathcal{T}_2), \ldots (\mathcal{E}_k, \mathcal{T}_k)\}$ where k is the number of contacts.

At supported postures, the body makes contacts with the support-surfaces. The location of a contact on the surface should be chosen such that the execution of the task is feasible and comfortable. Therefore, the location of the contact is computed through optimisation as a part of posture prediction. For this, the contact between surfaces needs to be modelled.

For any parametrically represented surface $S(u, v)$, the points on the surface are determined by two parameter values u and v. We attach a contact-site on a surface and parametrise the position of the site using the parameter values. Then, the origin of the frame will be a point on the surface, and the normal and a tangent vector at that point will complete the frame of reference. A third parameter ϕ would be required to control the rotation of the site about the normal. Now, the contact between surfaces can be established by using the site-parameters (u, v and ϕ) as optimisation variables and enforcing the kinematic constraint between the sites. Figure 2 shows the end-effector and target surfaces (E and T) before and after establishing contact.

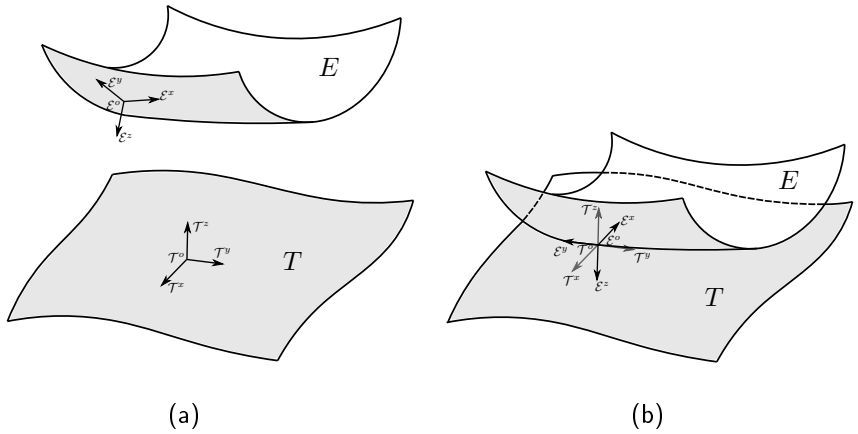

Figure 2: (a) End-effector and target surfaces with contact-sites defined (b) Contact surfaces after contact is established. Position and one of the orientations (z- axis) constraints are enforced on the contact-sites.

The support reaction forces (SRFs) are the contact forces at the support-points and will be determined through optimisation. It is required to develop a representation for the SRFs that can account for the friction at the contacts. As shown in Figure 3(a), we represent the force-vector $\mathbf{f} = (\alpha, \beta, m)$ using its direction α, β and magnitude (m). Let K be the line of action and K' be the projection of K on the xy- plane. Then α is the angle made by K' with x- axis, and β is the angle made by K with z- axis as shown in Figure 3(b). This representation allows modelling the friction cone by setting a range on the second Euler angle (β). Thus, $0 < \beta < \beta^*$, such that $\beta^* = tan^{-1}(\mu)$, where μ is the co-efficient of friction between the surfaces.

2.3 Stability Conditions

Let the ground-plane on which the primary support rests be represented by P and the normal to the plane be the unit vector $\hat{\mathbf{n}}$. Apart from the weight, the body also experiences the SRFs, and external loads due to the task. Let $\mathbf{F}$ be the resultant force acting through some reference point on the plane P, and $\mathbf{M}$ be the resultant moment. Now we resolve $\mathbf{F}$ and $\mathbf{M}$ into normal components $\overline{\mathbf{F}}_v$, $\overline{\mathbf{F}}_h$ and $\overline{\mathbf{M}}_v$, $\overline{\mathbf{M}}_h$ respectively.

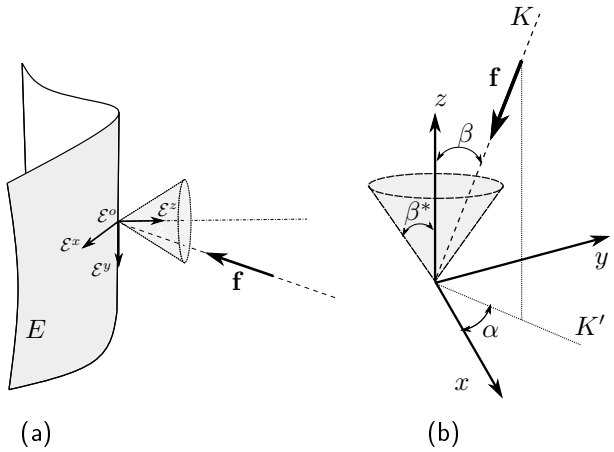

Figure 3: Modelling SRF and friction cone at a support-contact: (a) End-effector surface with contact-site $\mathcal{E}$ and SRF $\mathbf{f}$. (b) Representing the line of action (K) with respect to the site coordinate frame using Euler angles (α and β).

Then,

$$\overline{\mathbf{F}}_v = \mathbf{F} \cdot \hat{\mathbf{n}} \ , \ \overline{\mathbf{M}}_v = \mathbf{M} \cdot \hat{\mathbf{n}}$$

$$\overline{\mathbf{F}}_h = \mathbf{F} - \overline{\mathbf{F}}_v \ , \ \overline{\mathbf{M}}_h = \mathbf{M} - \overline{\mathbf{M}}_v$$

If we assume that both $\overline{\mathbf{F}}_v$ and $\overline{\mathbf{F}}_h$ exists, then the moments $\overline{\mathbf{M}}_v$ and $\overline{\mathbf{M}}_h$ can be cancelled out by transferring the lines of action of the force components. Then all the load acting on the body can be replaced by two forces $\mathbf{F}_v$ and $\mathbf{F}_h$ obtained by transferring $\overline{\mathbf{F}}_v$ and $\overline{\mathbf{F}}_h$ respectively. Since a vertical component would always exist due to the weight of the body, it is possible to replace the horizontal component of moment $\overline{\mathbf{M}}_h$ by transferring $\mathbf{F}_v$. The line of action of $\mathbf{F}_v$ intersects the ground-plane P at the Zero Moment Point (ZMP) $\mathbf{z}$. The first condition for stability requires the ZMP to lie inside the functional stability region (FSR) [8, 19] which is a region inside the Base of Support (BOS) of the primary-supporting segment. Enforcing this condition ensures that there are no unbalanced tipping moments.

However, unbalanced moments with axis normal to ground-plane P need to be checked. If there is no horizontal force component $\overline{\mathbf{F}}_h$, and a vertical moment component $\overline{\mathbf{M}}_v$ exists, then the moment cannot be eliminated, and the system would be unstable. When $\overline{\mathbf{F}}_h$ is non-zero, then the second condition for stability can be tested as follows.

On the contact surface of the primary support, two points $\mathbf{a}$ and $\mathbf{b}$ are identified as shown in Figure 4. When $\mathbf{z}$ is inside the FSR, a line through $\mathbf{z}$ parallel to the longitudinal median of the foot is taken, and the points $\mathbf{a}$ and $\mathbf{b}$ are chosen at the intersection of this line with posterior and anterior edges of the FSR respectively. The net vertical force $\mathbf{F}_v$, can now be resolved into parallel components $\mathbf{F}_v^a$ and $\mathbf{F}_v^b$ acting through $\mathbf{a}$ and $\mathbf{b}$ respectively, as shown in Figure 4b. The net horizontal force $\mathbf{F}_h$ is resolved into orthogonal components $\mathbf{F}_i$ and $\mathbf{F}_j$ as shown in Figure 4a. Let $\hat{\mathbf{r}}$ be the unit vector along $\mathbf{ba}$; then, $\mathbf{F}_j = \mathbf{F}_h.\hat{\mathbf{r}}$ and $\mathbf{F}_i = \mathbf{F}_h - \mathbf{F}_j$

Now, $\mathbf{F}_i$ is further resolved into parallel components $\mathbf{F}_i^a$ and $\mathbf{F}_i^b$ acting at $\mathbf{a}$ and $\mathbf{b}$ respectively. $\mathbf{F}_j$ is distributed between $\mathbf{a}$ and $\mathbf{b}$ by decomposing into $\mathbf{F}_j^a$ and $\mathbf{F}_j^b$ in the ratio of the corresponding vertical components $\mathbf{F}_v^a$ and $\mathbf{F}_v^a$

$$\frac{\mathbf{F}_j^a}{\mathbf{F}_j^b} = \frac{\mathbf{F}_v^a}{\mathbf{F}_v^b}$$

This step is shown in Figure 4(b).
Now, the net vertical and horizontal reaction forces at $\mathbf{a}$ and $\mathbf{b}$ are given by,

$$\mathbf{R}_v^a = -(\mathbf{F}_v^a)\ ,\ \mathbf{R}_v^b = -(\mathbf{F}_v^b)$$

$$\mathbf{R}_h^a = -(\mathbf{F}_i^a + \mathbf{F}_j^a)\ ,\ \mathbf{R}_h^b = -(\mathbf{F}_i^b + \mathbf{F}_j^b)$$

These reaction forces are shown in Figure 4(c). Then, the second condition of stability is given by,

$$\frac{\|\mathbf{R}_h^a\|}{\|\mathbf{R}_v^a\|}, \frac{\|\mathbf{R}_h^b\|}{\|\mathbf{R}_v^b\|} \leq \mu \tag{1}$$

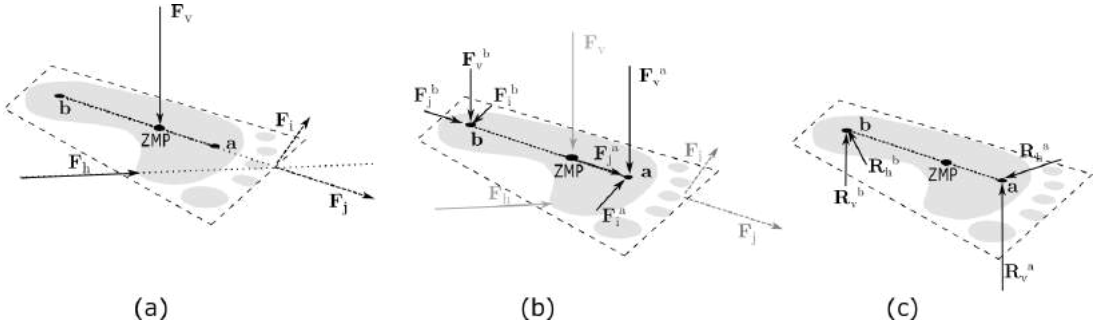

Figure 4: Resolving Ground Reaction forces and evaluation of stability. (a) The net vertical and horizontal forces acting on the body (b) Net vertical and horizontal forces distributed between points $\mathbf{a}$ and $\mathbf{b}$. (c) Vertical and horizontal reactions at points $\mathbf{a}$ and $\mathbf{b}$.

2.4 Joint Stress

In order to maintain a given posture in the presence of the weight of the body-segments and external loads, the muscles in the body generate forces that produce moments about different joints. The validity of the predicted posture also depends on whether the biomechanical stress acting on the body is acceptable. In our model, we compute the torque acting on each joint and resolve it into components that correspond to different modes of rotation of the joint such as flexion, abduction, and medial-rotation as described in [7, 19]. The joint torque components are normalised with their respective maximum torque capacity. For example, if vector $\mathbf{T}_i$ represent the torque acting on i^{th} joint, it is resolved into three components, $\mathbf{T}_i^x$,$\mathbf{T}_i^y$ and $\mathbf{T}_i^z$. With τ_i^x,τ_i^y and τ_i^z representing the torque capacities, the normalised torque components are, λ_i^x,λ_i^y and λ_i^z such that $\lambda_i^* = \frac{\|\mathbf{T}_i^*\|}{\tau_i^*}$, where $*$ can be any of x, y or z.

The normalised torque can be constrained to lie within a limiting percentage value representing the allowable level of exertion. The net joint effort λ_i is defined as,

$$\lambda_i = \sqrt{\frac{(\lambda_i^x)^2 + (\lambda_i^y)^2 + (\lambda_i^z)^2}{3}}$$

A measure of overall postural effort is also defined based on the individual joint stress values [19].

$$\lambda_{overall} = \sqrt{\sum_{i=1}^{N} \lambda_i^2}$$

2.5 Optimization Formulation

The mathematical formulation of the optimisation problem is described below.

2.5.1 Decision-Variables

As the optimisation computes the posture, contact-location and the SRFs together, the decision-variables are represented by vector $\mathbf{x}$ that includes the joint angle vector θ, the position vector of contacts $\mathbf{p}$ and the support reaction force vector $\mathbf{f}$.

$$\mathbf{x} = [\theta^T \mathbf{p}^T \mathbf{f}^T]^T \tag{2}$$

The vectors θ,$\mathbf{p}$ and $\mathbf{f}$ are individually defined as follows:

$$\theta = [\theta_1\ \theta_2\ \theta_3\ \ldots\ \theta_n]^T \tag{3}$$

$$\mathbf{p} = [\mathbf{p}_1^T\ \mathbf{p}_2^T\ \ldots\ \mathbf{p}_k^T]^T \tag{4}$$

$$\mathbf{f} = [\mathbf{f}_1^T\ \mathbf{f}_2^T\ \ldots\ \mathbf{f}_k^T]^T \tag{5}$$

θ represents the pose of the body, where θ_i are joint angle values, and n is the total degrees of freedom pertaining to joints.

The vector $\mathbf{p}$ carries the variables deciding the contact-locations, where $\mathbf{p}_i$ holds the surface-parameter values at i^{th} contact and k is the number of contacts.

$\mathbf{f}_i$ is the force-vector acting at i^{th} contact as described in Section 2.2.

2.5.2 Constraints

Kinematic-constraints:
The set of kinematic-constraints is represented by the list of contact-site pairs
$C = \{(\mathcal{E}_1, \mathcal{T}_1), (\mathcal{E}_2, \mathcal{T}_2), \ldots (\mathcal{E}_k, \mathcal{T}_k)\}$ as described in Section 2.2. A contact constraint can be defined for position and orientation per contact. For a contact i, the position constraint is defined by,

$$\mathcal{E}_i^o = \mathcal{T}_i^o \tag{6}$$

By representing the co-ordinate axes of contact-sites with unit vectors, orientation constraints can be defined using the dot products of two corresponding co-ordinate axes.

$$\mathcal{E}_i^z \cdot \mathcal{T}_i^z = -1\ ,\ \mathcal{E}_i^x \cdot \mathcal{T}_i^x = -1 \tag{7}$$

The constraints are applied for all $i = 1, 2, \ldots, k$

Other than the constraints required to enforce the contact, the bounds on the parameters controlling the contact-sites are included as constraints.

Stability-Constraints:
Let g be the signed distance of $\mathbf{z}$ from FSR. In Figure 5 the FSR is shown as a quadrilateral in bold lines. The distance is negative if $\mathbf{z}$ is inside and positive if $\mathbf{z}$ is outside the polygon [19]. Thus the constraint is represented by the inequality,

$$g(\mathbf{x}) < 0 \tag{8}$$

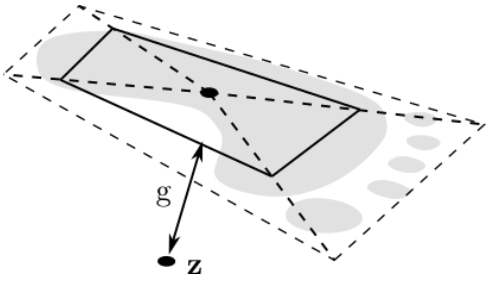

Figure 5: The Base of Support of primary-supporting foot showing FSR (bold line), Zero Moment Point $\mathbf{z}$ and the distance function g.

The second stability condition requires the computed GRF vector at the support to lie within the friction cone. This requirement is captured by the constraint equation 1.

Additionally, the limits on the Euler-angle controlling the SRF are included to enforce the constraint representing the friction cone as described in Section 2.2.

Joint-Constraints:
There are two types of constraints associated with joints, namely the range of motion constraints on the joint-angles and the joint-strength constraints to limit the torques.
For the i^{th} degree-of-freedom(DOF) of the joint-angle vector θ,

$$\theta_i^L < \theta_i < \theta_i^U, \quad \forall \quad i = 1, 2, \ldots, n \tag{9}$$

where θ_i is the joint angle value, θ_i^L is the lower limit, and θ_i^U is the upper limit on the range of motion.

A limiting value on normalised joint torque is set for each joint.

$$\lambda_i^x, \lambda_i^y, \lambda_i^z < \lambda_{max} \quad \forall \quad i = 1, 2, 3, \ldots, N \tag{10}$$

where, λ_i^x, λ_i^y and λ_i^z are the components of efforts in different axes of rotation and, λ_{max} represent the limit such that, $0 < \lambda_{max} < 1$. N is the number of joints.

2.5.3 Objective Functions

The posture-prediction is performed over three stages of optimisation. In the first stage, the kinematic constraints are enforced using inverse kinematics. At this stage, only the joint angle values (eq.3) and contact-location variables (eq.4) are used as decision-variables. The sum of violations of kinematic constraints is used as the objective function as defined below.

$$z_1 = \sum_{i=1}^{k} (w_1 \|\mathcal{E}_i^o - \mathcal{T}_i^o\|^2 + w_2 \|\mathcal{E}_i^z - \mathcal{T}_i^z\|^2 + w_3 \|\mathcal{E}_i^x - \mathcal{T}_i^x\|^2)$$

where,w_1, w_2 and w_3 are weights to scale the values to comparable range.

In the second stage, the stability requirements are enforced while imposing kinematic-constraints (eq.6,7) achieved in the previous stage. At this stage, all the decision-variables are used (eq.2), and the sum of violations of stability constraints is used as the objective function.

$$z_2 = w_4 G_{zmp} + w_5 G_{grf}$$

where G_{zmp} represents zero moment point violation defined by,

$$G_{zmp} = \begin{cases} g(\mathbf{x})^2 & \text{if } g(\mathbf{x}) > 0 \\ 0 & \text{otherwise} \end{cases}$$

G_{grf} represent the violation of friction limits by GRFs,

$$G_{grf} = G^a_{grf} + G^b_{grf}$$

such that,

$$G^x_{grf} = \begin{cases} (\frac{\|\mathbf{R}^x_h\|}{\|\mathbf{R}^x_v\|} - \mu)^2 & \text{if } \frac{\|\mathbf{R}^x_h\|}{\|\mathbf{R}^x_v\|} > \mu \\ 0 & \text{otherwise} \end{cases}$$

where x represents point a or b as described in Section 2.3. w_4 and w_5 are co-efficients for scaling.

In the third stage, the final posture is determined by using all decision-variables and constraints while minimising a weighted sum of human performance measures.

$$z_3 = w_6\lambda_{overall} + w_7 H_{jointdev} + w_8 H_{symmetry}$$

Here, $\lambda_{overall}$ is the overall biomechanical postural stress defined in Section 2.4. $H_{jointdev}$ is the measure used to minimise the joint-angles deviation from the nominal value, and $H_{symmetry}$ is used to enforce symmetry between the left and the right sides of the body.

$$H_{jointdev} = \sum_{i=1}^{n} |\theta_i - \theta_i^N|^2 \text{ and } H_{symmetry} = \sum_{i=1}^{n} |\theta_i - \theta_i^*|^2$$

where θ_i^N represents the nominal angle value for i^{th} joint-DOF, and it corresponds to the joint angle value at normal standing posture. θ_i^* is used to denote the corresponding contra-lateral joint-DOF for θ_i. For example, the right knee-flexion angle corresponds to the left-knee flexion. Note that contra-lateral joints are not defined for torso, neck and head joints. In the current model, the values for weights were assigned as follows $w_6 = 0.8$,$w_7 = 0.1$ and $w_8 = 0.1$ when simulating symmetric tasks like sitting. For a generic task, the values are set as $w_6 = 0.9$,$w_7 = 0.1$ and $w_8 = 0$

The optimisation problems are solved using the Sequential Quadratic Programming (SQP) algorithm [15] from the NLopt library [11].

3 SUPPORT-SELECTION

In this section, we first develop a rationale for selecting support-surfaces by examining the mechanics of support-taking. Then we propose a three-stage procedure for generating the set of support contacts from the objects available in the environment for executing the given task. As it is possible to perform the same task with different combinations of support, multiple contact-sets $C_1, C_2, \ldots C_m$ will be generated so that m different postures corresponding to alternate modes of taking support can be computed for performing the same task.

3.1 Mechanics of Support-Taking

It is reported in the literature that there are three major ways in which support-taking enhances performance, namely, the extension of maximum reach, increase in force-exertion capability, and reduction of spinal-loading. We examine the mechanical aspects of these effects as follows.

We know that, for a posture to be stable, it is necessary that the zero moment point (ZMP) lies inside the base of support (BOS) of the body. For reach tasks, no external loads act on the body; therefore, the ZMP and ground projection of the centre of mass (GCOM) will be the same. During extreme reach efforts, the body leans towards the reach-target resulting in GCOM moving out of the BOS, and the posture becomes unstable. When a support is taken, the SRF can produce a restoring couple with the GRF and counter the tipping moment. Thus it enhances the reach without compromising stability.

For exertion tasks, the GCOM and ZMP are different. Here, the external forces and moments incurred due to the exertion task can displace the ZMP out of the BOS. As seen in the case of reach tasks, taking support can help in generating a restoring moment so that the ZMP is brought inside the BOS when it goes out. Thus, support-taking improves the capability to exert load by helping in maintaining balance. Other than that, it has been observed in [6] that leaning towards the target can improve the exertion capability of the arm because it may favour an elbow-angle that is optimal for exertion.

For tasks that require torso-flexion, the torso-joint develops a large torque due to the weight of the upper-body. If the task involves carrying weight, the moment due to the carried weight also adds to the torque. In such scenarios, taking support with the non-task hand will help generate a counter-moment, thereby reducing the torque at the torso-joint. Thus taking support reduces the loading on the spine by redistributing the joint torques.

From the above discussion, we see that the main purpose of taking support is to obtain a counter-moment provided by the SRF, be it for restoring balance or reducing spinal loading. Therefore, we start the support-selection process by identifying support-surfaces from which we can draw SRFs, that can produce the required counter-moment. We refer to these surfaces as feasible support-surfaces or simply feasible supports. The feasible supports that can be reached by a supporting body-segment are called reachable supports. As there can be multiple reachable supports for a given body-segment, multiple supported postures can be generated for the same task. Thus, multiple contact-sets $C_1, C_2, \ldots C_m$ for different support-modes with different combinations of contact-pairs will be generated. The procedure outlined above is described in detail in three stages, as follows.

3.2 Selecting Feasible Support-Surfaces

We know that the counter-moment is produced by the couple formed by an SRF and a component of the GRF. In order to produce the required moment-vector, the SRF-vector should have the right direction, point-of-application and magnitude, assuming that the accompanying GRF component can always be availed. Then, it is possible to imagine infinitely many configurations for the SRF-vector that can produce the required moment-vector. Since the magnitude of the SRF will be decided by optimisation, we are required to find only the suitable directions and points-of-application of the SRFs that can be provided by the available surfaces. The procedure for selecting the feasible supports, is elaborated below.

3.2.1 Estimation of Counter-Moment

To determine if a support is indeed necessary, the task is first simulated without considering support as the stability constraint. If the predicted posture violates the ZMP condition for stability, we say that support-taking is required for maintaining balance. Likewise, if the joint-stress developed at the torso-joint is above a specified threshold value, then support-taking is required to reduce spinal loading. Since the magnitude of the SRF is determined through optimisation, finding the direction of the moment-vector alone is sufficient for identifying the surfaces that can offer the required support.

In case of support-taking to maintain balance, the ZMP of the posture computed without support will be lying outside the BOS. Now, the axis of the counter-moment will be given by the edge of the BOS that is nearest to the ZMP. Let $\mathbf{z}$ be the position of ZMP, $\mathbf{b}$ be a point on the nearest edge that is closest to $\mathbf{z}$ and

$\hat{\mathbf{n}}$ be the normal vector of the ground-plane. Then, the axis of counter-moment $\mathbf{a}$ is given by,

$$\mathbf{a} = (\mathbf{z} - \mathbf{b}) \times \hat{\mathbf{n}}$$

The direction of the counter-moment is the unit vector $\hat{\mathbf{a}}$ obtained by normalising $\mathbf{a}$. Here, the point $\mathbf{b}$ is referred to as pivot-point.

For the case of reducing spinal-loading, the axis of counter-moment $\mathbf{a}$ is opposite in direction to the axis of torque acting at the torso-joint. In this case, the pivot-point $\mathbf{b}$ corresponds to the location of the torso-joint.

3.2.2 Identification of Feasible Directions

For producing a moment about an axis, a force should have a component perpendicular to the axis (assuming a non-zero moment arm). Therefore, directions that are predominantly perpendicular to $\hat{\mathbf{a}}$ are considered for SRFs. That is $|\hat{\mathbf{x}} \cdot \hat{\mathbf{a}}| < \epsilon_0$, where $\mathbf{x}$ is a direction of SRF and ϵ_0 is a tolerance to permit some deviation allowed by friction. The set of feasible directions S, satisfying this condition is represented by,

$$S = \{\hat{\mathbf{x}} : \ \ |\hat{\mathbf{x}} \cdot \hat{\mathbf{a}}| < \epsilon_0\}$$

3.2.3 Selection of Surfaces

In the current work, the surfaces chosen for support-taking are limited to planar and cylindrical surfaces and are denoted by $\mathcal{F}^p$ and $\mathcal{F}^c$ respectively. The objects in the present model were represented as mesh, and the surfaces were computationally extracted from the mesh model using the methods described in [20]. The bounded planar and cylindrical faces extracted from the mesh are referred to as support-features.

Planar features: A planar feature $\mathcal{F}^p$ is represented using the set of bounding polygons and a normal-vector. The bounding polygons are represented by sets of vertices and edges. For a planar feature $\mathcal{F}^p$, $\hat{\mathbf{n}}(\mathcal{F}^p)$ shall denote the function returning the unit-normal vector, while $V(\mathcal{F}^p)$ shall denote the set of all the vertices forming the bounding polygons.

Cylindrical features: A cylindrical feature $\mathcal{F}^c$ is represented using the value of its radius and a line segment that denotes the bounded axis of the cylinder. Let $r(\mathcal{F}^c)$ denote the radius, $\hat{\mathbf{a}}(\mathcal{F}^c)$ be the direction of the cylinder's axis, and $\mathbf{v}_1(\mathcal{F}^c)$ and $\mathbf{v}_2(\mathcal{F}^c)$ denote the vertices bounding the axis.

Since the environment may include features that are located far away from the subject, we select the available features for the cylindrical and planar features that are present in the vicinity of the DHM. We denote these sets of short-listed cylindrical and planar features as $F^c = \{\mathcal{F}_i^c\}$ and $F^p = \{\mathcal{F}_i^p\}$ respectively. These features are selected if they are located within a threshold distance from the DHM's local reference point (centre of the pelvis).

Selection criteria: The point on a support-feature where the contact is made is called the support-point. The SRF offered by a support-point is predominantly in the direction of the normal-vector of the surface at that point. Although the surface-friction offers a tangential component to the SRF, it is a function of the magnitude of the normal component. Therefore, we can say that a support-feature should have at least one point with normal-vector that belongs to the set S. However, the ability to provide an SRF in the feasible direction is only a necessary condition and is not sufficient. If a support-feature has to offer an SRF that can produce the required counter-moment, the location of the support-point on the feature needs to be valid with respect to the pivot-point $\mathbf{b}$ and the direction of counter-moment $\hat{\mathbf{a}}$. For a point on a support-feature to be a valid support-point, it should satisfy the following condition.

Let $\mathbf{s}$ be a point on the feature and $\mathbf{v}$ be the surface-normal at that point. Let A be a line that represents the axis of the counter-moment passing through the pivot-point $\mathbf{b}$. Then, the direction of A would be given by

$\hat{\mathbf{a}}$. Now, let the point $\mathbf{s}^*$ be the projection of $\mathbf{s}$ on the line A, given by $\mathbf{s}^* = \mathbf{b} + p\hat{\mathbf{a}}$, such that $p = (\mathbf{s} - \mathbf{b}) \cdot \hat{\mathbf{a}}$. Then, the point $\mathbf{s}$ is said to be valid if the following condition holds.

$$((\mathbf{s} - \mathbf{s}^*) \times \mathbf{v}) \cdot \hat{\mathbf{a}} > 0 \tag{11}$$

If a support-feature has at least one point whose normal-vector belongs to S and is valid as per eq(11), then it is a feasible support.

Selecting Planar features: A planar feature $\mathcal{F}^p$ is feasible if the normal-vector belongs to S and at least one point on the planar face is valid. That is, $\hat{\mathbf{n}}(\mathcal{F}^p) \in S$ and at least one of the vertices in $V(\mathcal{F}^p)$ is valid as per eq(11). Figure 6 illustrates the selection of planar supports for the task of leaning forward. Completing this task requires a counter-moment whose direction is normal to sagittal-plane, pointing from left to right of the DHM. The pivot-point $\mathbf{b}$ and the normal-vector of ground-plane $\mathbf{n}$ are also shown in the figure. In Figure 6(a), representatives of planar features from all possible positions and orientation are shown. Since the direction of counter-moment is normal to sagittal-plane, only planar feature with normal-vectors parallel to the sagittal-plane are feasible. For a reach-task that requires the human to lean forward, the planar features shown in 6b are feasible supports.

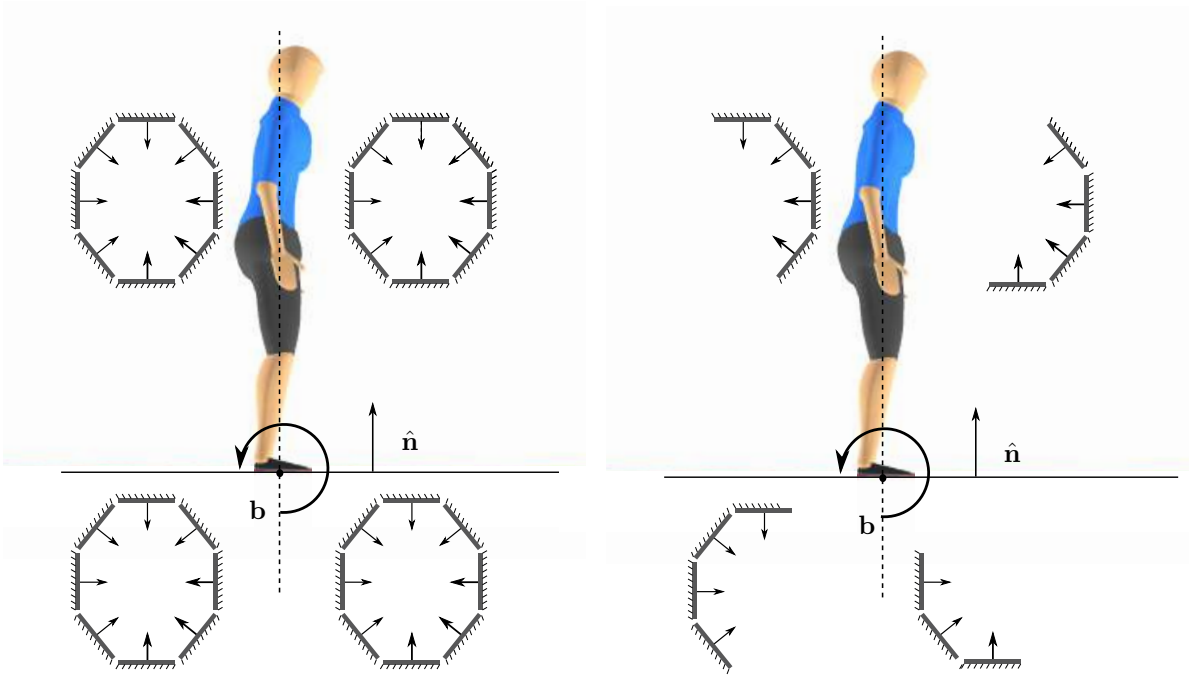

(a) (b)

Figure 6: Selecting planar features based on surface normals and location for generating an anti-clockwise counter-moment(a)Representative planar features shown at different possible positions and orientations. (b) planar features that can offer the required counter-moment.

Selecting Cylindrical features: For cylindrical surfaces, normal reactions can be obtained in all directions that

are perpendicular to the axis of the cylinder. While the cylinders can be arbitrarily oriented in the space, in this work, only the cylindrical features of specific orientations are considered for taking support. These features are classified into two sets and are described below.

1. Set of cylindrical features whose axes are almost parallel to the axis of counter-moment.

$$F_1^c = \{\mathcal{F}^c \in F^c : |\hat{\mathbf{a}}(\mathcal{F}^c) \cdot \hat{\mathbf{a}}| < 1 - \epsilon_0\}$$

. In Figure 7 these cylindrical surfaces are shown as circles.

2. Set of cylindrical features whose axes are almost perpendicular to the axis of counter-moment.

$$F_2^c = \{\mathcal{F}^c \in F^c : |\hat{\mathbf{a}}(\mathcal{F}^c) \cdot \hat{\mathbf{a}}| < \epsilon_0\}$$

In Figure 7, these cylinders are shown as shaded rectangles.

Now, the condition for feasibility needs to be established separately for the two sets F_1^c and F_2^c.

Any cylindrical feature $\mathcal{F}_c \in F_1^c$, will have a normal vector in S. This is because the axis of the cylinder is parallel to $\hat{\mathbf{a}}$ and the curved surface can offer SRFs in all directions normal to $\hat{\mathbf{a}}$. The validity condition for features contained in F_1^c is as follows.

For a given $\mathcal{F}_c \in F_1^c$, we first compute $\mathbf{v}^*$ by projecting either $\mathbf{v}_1(\mathcal{F}^c)$ or $\mathbf{v}_2(\mathcal{F}^c)$ on A. After that, we define a vector $\mathbf{k} = \hat{\mathbf{a}} \times (\mathbf{v}_1(\mathcal{F}^c) - \mathbf{v}^*)$ and the feasible SRF directions as $S_1 = \{\hat{\mathbf{x}} : \hat{\mathbf{x}} \cdot \hat{\mathbf{k}} > 1 - \epsilon_1\}$, where $\hat{\mathbf{k}}$ is the unit-vector along $\mathbf{k}$. Now, the cylindrical feature $\mathcal{F}_c$ is valid if $S \cap S_1 \neq \emptyset$. Additionally, the condition $\|\mathbf{v}_1(\mathcal{F}^c) - \mathbf{v}^*\| > r(\mathcal{F}_c)$ should be checked to ensure that A lies outside the volume of the cylinder.

We test the feasibility of features contained in F_2^c as follows. For a given cylindrical feature $\mathcal{F}^c \in F_2^c$, there is a single direction that will be normal to both $\hat{\mathbf{a}}$ and $\hat{\mathbf{a}}(\mathcal{F}^c)$. This direction is given by $\hat{\mathbf{h}} = \hat{\mathbf{a}} \times \hat{\mathbf{a}}(\mathcal{F}^c)$. The feasible normal-vector on the surface is $\hat{\mathbf{h}}$ if $\hat{\mathbf{h}} \in S$ and $-\hat{\mathbf{h}}$ if $\hat{\mathbf{h}} \notin S$. The validity condition holds for all $\mathcal{F}^c \in F_2^c$, since there will always be a point on the curved surface of the cylinder with either $\hat{\mathbf{h}}$ or $-\hat{\mathbf{h}}$ as surface normal.

In Figure 7 the representatives of cylindrical features in all possible positions and orientations are shown. Here, the normal vectors that are not feasible are shown in dashed lines.

3.3 Selecting Reachable Support-Surfaces

Since not all feasible supports will be reachable by the supporting body segments, it is required to identify the set of feasible supports that a body segment can reach. In the current work, the body segments that are considered for taking support are the hand and foot.

The first condition to be satisfied for both hand and foot supports is that at least a part of the feasible support should be within the workspace of the support-taking limb (arm or leg). This requirement is expressed as follows.

$$d_{sup}^L < d(\mathbf{j}, \mathcal{F}) < d_{sup}^U$$

Here, $d(\mathbf{j}, \mathcal{F})$ gives the distance of the feature $\mathcal{F}$ from the position $\mathbf{j}$ of the joint driving the limb (hip for leg and shoulder for arm). d_{sup}^L and d_{sup}^U are lower and upper thresholds of reach distances of the limb. For foot support, d_{sup}^U is the sum of lengths of the femur and tibia segments, and d_{sup}^L is the difference in the lengths. Similarly, for hand support, the lengths of the upper and forearm are used to define d_{sup}^L and d_{sup}^U.

The second condition requires that at least a part of the feasible support is on the ipsilateral side of the supporting segment. This condition is tested as follows. The bounding vertices of the features ($V(\mathcal{F})$ are first transformed with respect to the DHM's local frame of reference $\mathcal{L}$ (described in 2.1). As the z axis of the frame $\mathcal{L}_z$ represents the right-hand side of the DHM, we can say if a feasible support is suitable for right hand

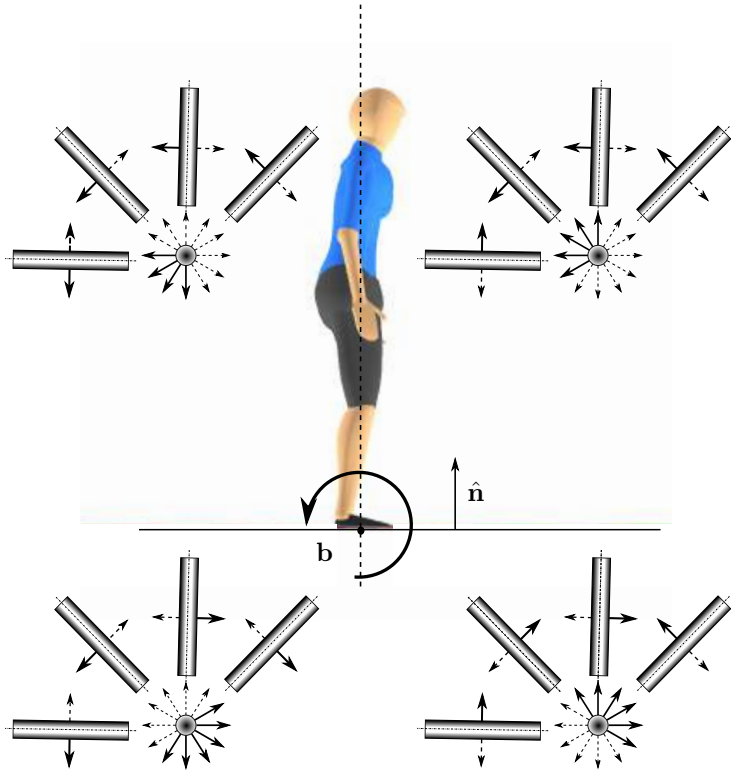

Figure 7: Representative cylindrical features are shown at different possible positions and orientations. Infeasible normal vectors are shown in dashed line.

or foot by testing if there is at least one transformed bounding vertex with positive z-coordinate. Likewise, for the left hand and foot, the feature should have at least one vertex with a negative z-coordinate.

Now we look at the conditions that are applied specifically for hand and foot supports. For foot support, firstly, the support feature should be located below the waist height. This condition is tested by checking if there is at least one transformed bounding vertex that has a negative y-coordinate. Secondly, for a foot support to use a planar feature, the plane should be normal to the sagittal plane and face the body. These conditions are expressed as follows.

$$|\hat{\mathbf{n}}(\mathcal{F}^p) \cdot \mathcal{L}_z| < \epsilon_4 \text{ and } \hat{\mathbf{n}}(\mathcal{F}^p) \cdot \frac{\mathbf{x}}{\|\mathbf{x}\|} > (1 - \epsilon_5)$$

where, $\mathbf{x} = (\mathcal{L}_o - \mathbf{p}(\mathcal{L}_o, \mathcal{F}^p))$, such that, $\mathbf{p}(\mathcal{L}_o, \mathcal{F}^p)$ is the projection of $\mathcal{L}_o$ on plane $\mathcal{F}^p$, and ϵ_4 and ϵ_5 are small positive tolerance values.

For hand supports, the support feature cannot be located at a very low height as it would require the human to bend down and assume an unnatural posture. Therefore, there should be at least a part of the feature above a threshold height. Here, the knee-height is taken as the threshold height. The condition is checked by testing if there is at least one transformed bounding vertex of the feature with a y-coordinate above the value corresponding to the knee-height.

3.4 Generating Support Contacts

With the reachable features for each supporting segment identified, now we see how to generate the set of support contacts $C = \{(\mathcal{E}_1, \mathcal{T}_1), (\mathcal{E}_2, \mathcal{T}_2), \ldots (\mathcal{E}_k, \mathcal{T}_k)\}$ that represents the kinematic targets of a supported posture. To get multiple supported postures, alternate contact sets $C_1, C_2, \ldots C_m$ will be created.

Firstly, the body segments that will be used for taking supports need to be identified. The hand or the foot other than the task hand and the root segment can be used for taking support. For the support segments, the end-effector site is already created at designated locations, namely the palm of the hand and sole of the foot. For assuming alternate postures, the same segment can take support on different surfaces or at different locations on the same surface. Therefore it is required to create multiple target sites on the reachable support surfaces corresponding to each support-segment.

For creating target sites, it is required to decide the initial location of the target site on the support surface. Then, it is required to create a region around the target site on the surface that will define the bounds of the site. The initial location should be chosen such that it is easily reachable by the supporting segment while executing the task. Therefore, first, the posture for executing the given task without taking support is computed, and then a point on the surface that is near to the reaching limb is selected. The near point is obtained by projecting the position of the driving joint of the supporting limb on the surface. The driving joint for hand and foot supports are the shoulder and hip, respectively. Thus the position of a joint is projected on different reachable surfaces to obtain the locations for the target sites. For a planar feature, if the projected point is outside the bounds of the surface, multiple target sites are created on the surface on the bounding edges by re-projecting the point on different edges. For this x edges are selected by ranking all the edges based on their distance from the projected point and selecting the first x ranked edges.

The bounds of the support regions are computed by optimisation. For a given feature, a rectangular sub-domain is created per target site, and its bounding vertices are obtained by optimising for maximum area. The constraints for this optimisation require the location of the target site to be inside the domain and vertices of the domain to be within the bounds of the feature. Figure 8 shows the optimised support regions for different initial target-site locations on the same planar feature.

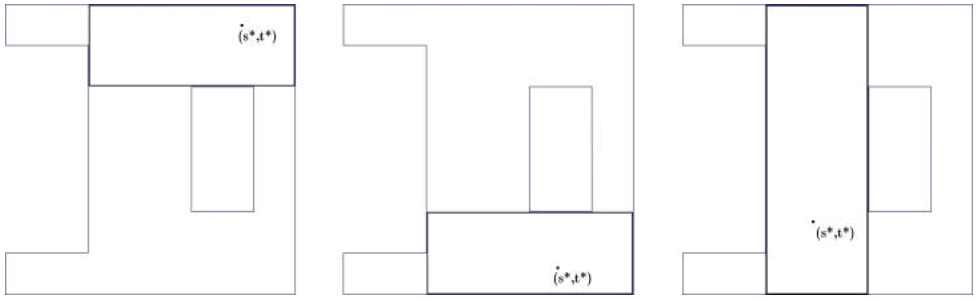

Figure 8: Expected maximised support region (rectangle in black colour) around three different target-site locations (s^*, t^*) for the same polygon. The bounding polygons of planar support feature are shown in blue.

After the target sites and their corresponding support regions are generated, different combinations of end-effector and target sites can be paired, and support contact sets $C_1, C_2, \ldots C_m$ can be created.

4 SIMULATION RESULTS

In this section, we present simulation examples for two task scenarios to demonstrate the automatic generation of supported postures using the proposed framework, namely one-handed reach and assisted sitting. We also present the evaluation of the postures from a biomechanical perspective. The simulations are created and

performed with the help of the graphic user interface (GUI) that was developed along with the DHM system. For creating the simulations, the models are imported into the environment, and the reach tasks are defined by specifying the end-effector and target sites, through the GUI.

4.1 Simulation of One-handed Reach With Support

The task here is to reach an object with the right hand while taking support with the non-task hand and foot. The object to be reached was placed on a table, and a box was placed on the floor between the table and the DHM, as an obstacle. The system automatically recognised the top horizontal surfaces of the box and table as support-features and used them to create supported postures. Figure 9(a) shows the posture computed for reaching the target without taking support. Figure 9(b) shows the reach-posture with foot using the box as support. Figure 9(c) shows the posture with both hand and foot as support, where the hand takes support on the table and the foot on the box. To understand the effect of support on the postural comfort, we

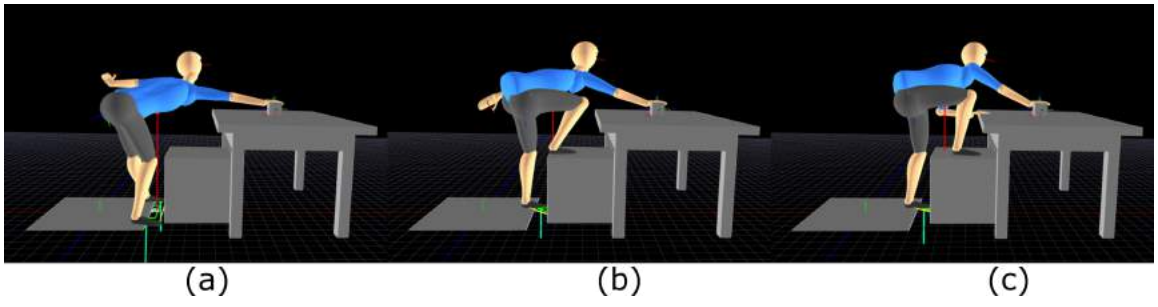

Figure 9: Different postures computed for one-handed reach-task with planar horizontal supports: a) reaching without support,b) foot support only c) foot as well as hand support

the individual joint-stresses λ_i and overall postural-effort $\lambda_{overall}$ (described in Section 2.4) for the generated posture are compared. In Figure 10 we can see that, while reaching without support, the joint-stress at the

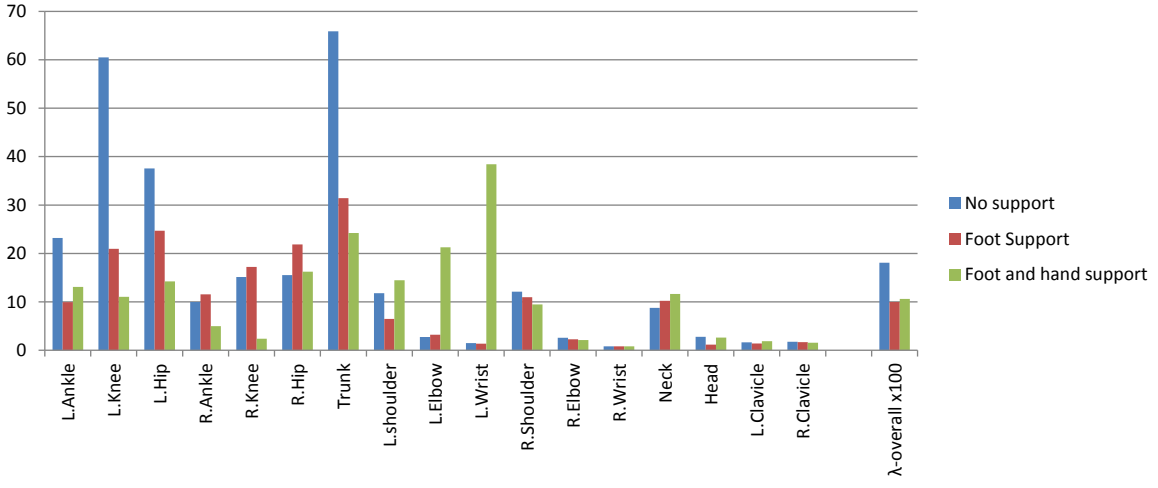

Figure 10: Comparison of postural efforts in three modes of reaching a) without support,b) foot support c) foot plus hand support

torso-joint is very high. Following the torso joint, high joint-stresses can be observed in the lower body joints on the left-hand side. This is possibly due to the torso leaning towards the left to facilitate reaching with the right hand. In contrast, the plots for the supported postures show that these joint-stresses are substantially reduced. In particular, we can see that the case of dual support reduces the joint-stresses on the lower body and torso but increases it on the joints of the left arm. The comparison of the overall postural effort shows that support-taking provides a significant biomechanical advantage.

In the second reach task, the reach-target was placed inside a constrained workstation as shown in Figure 11. Here, the system identified both horizontal and vertical support-surfaces and generated postures. Those taking support on vertical support-surfaces alone are shown in Figure 11. Here, it can be seen that the DHM

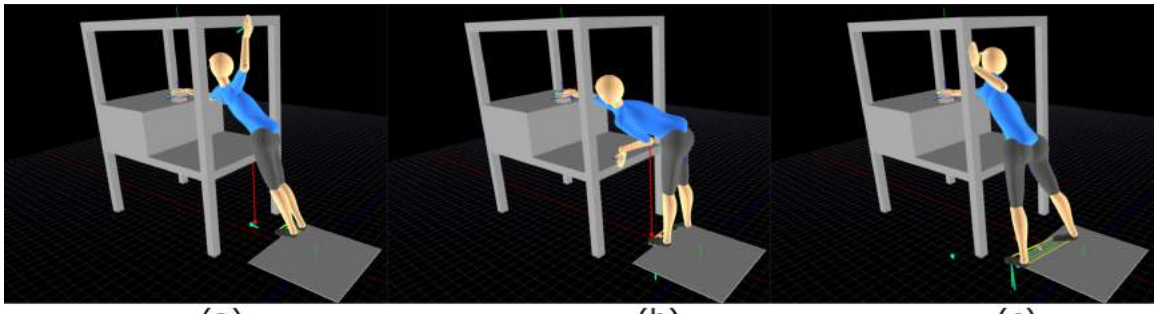

Figure 11: Different postures generated for one-handed reach-task using planar vertical support: support taken on a) top edge b) bottom edge c) side edge

is taking support at different locations on the same planar face in front.

4.2 Simulation of Assisted Sitting

Sitting is modelled here as a reach-task, where the hip acts as the end-effector and the seat as the reach-target. A sitting task may be accompanied by support-taking because, during sitting, the knee-joints experience high loading and taking support reduces the stress on the knees till the pelvis makes contact with the seat. Thus the decision to take support is made by assessing the stress at the knee-joints while sitting without supports. Here, we present two cases of assisted sitting. In the first case, the DHM is instructed to reach the surface of the chair with the pelvis, where the chair is provided with arm-rests. The system automatically recognised the arm-rest surfaces as supports and used them as supports for achieving the seated posture. Figure 12(a) shows the posture of the DHM while standing and after sitting with arm-rest supports. Although the system generated multiple modalities of assisted sitting, such as using only one arm-rest as support, only the natural two-handed assisted sitting posture is shown here. In the second case, the DHM is instructed to sit on a box. Here, instead of arm-rests, a horizontal cylindrical bar is provided in front of the DHM. Correspondingly a sitting posture that takes support on the cylindrical feature was generated. Figure 12(b) shows the standing posture and computed seated-posture that is taking support on the cylindrical bar with both hands.

5 DISCUSSION

The framework presented has addressed two major challenges, namely, the prediction of supported postures and the selection of appropriate supports. Computing supported postures even when the supports to be taken are provided, is challenging because the system is statically indeterminate. While existing models like [10] compute supported postures, by optimising the support reaction forces, they require the exact support-point

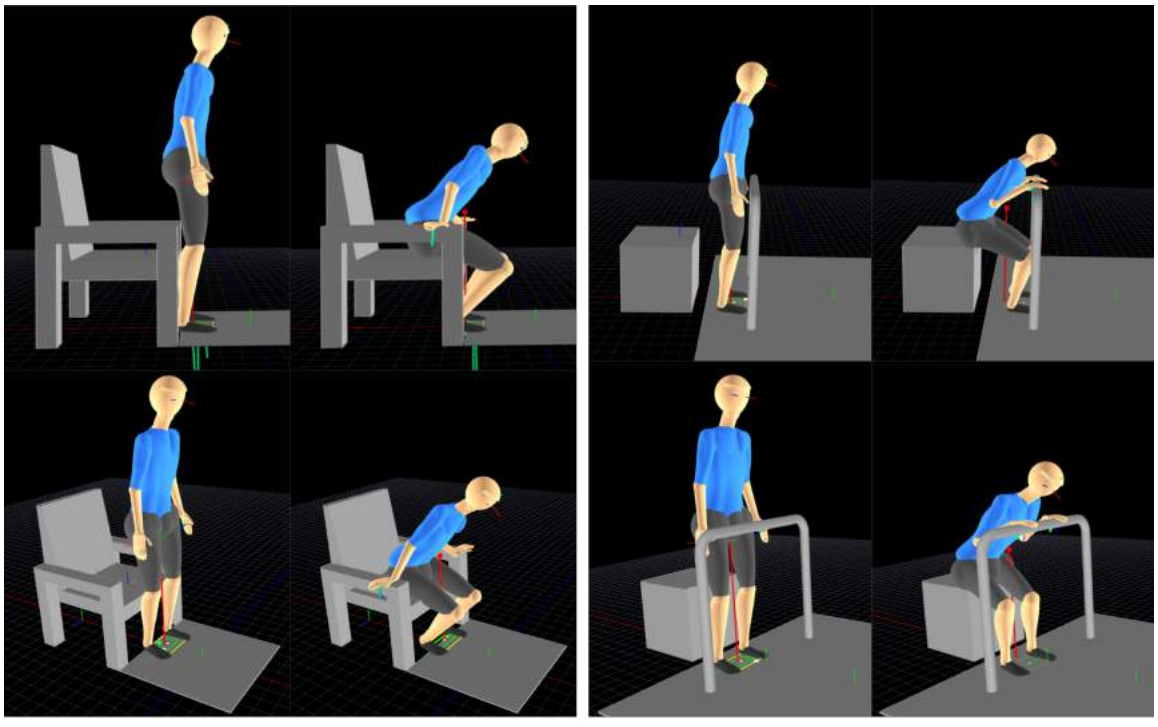

Figure 12: Sitting with support (a) chair with armrest (b) box with cylindrical railing in front.

to be provided. However, the proposed model takes the support-surface as input and computes the location of the support as well as the reaction force through optimisation. In addition to that, the designer can also specify the co-efficient of friction at support-contacts to get supported postures that satisfy friction constraints. This capability is mainly a consequence of the novel scheme used by the present model to represent support-contacts and contact-forces.

The other novel aspect of the proposed framework is the ability to automatically identify suitable support-surface based on the task to be performed. This allows the generation of multiple modalities of performing the same task. However, as the number of available support-surfaces increases, there will be more combinations causing the system to generate a large number of supported postures. Even though the generated postures may be valid according to modelled constraints, many of the generated postures may be impractical or unrealistic. Therefore, the designer will be required to choose the meaningful postures. Future models should incorporate more conditions to eliminate unnatural postures. Moreover, the supported postures generated by the current framework are not collision-free. Therefore the inclusion of collision-avoidance is deemed to be necessary.

The support surfaces considered in the current work are limited to planar and cylindrical surfaces. In future, support-taking on free-form surfaces may be explored. As the current model assumes that the support surfaces are parametrically represented, capabilities such as modelling contacts and computing support-region by optimisation can be extended to parametrically represented free-form surfaces as well. However, applying the model to parametric free-form surfaces will significantly increase the computational cost and performance, which needs to be addressed.

6 SUMMARY AND CONCLUSION

Human operators performing tasks while leaning or bracing on the surrounding structures is a commonly observed phenomenon in industries. Simulation of tasks involving supported postures using the existing DHM systems is cumbersome because the designer is required to manually select the support-surfaces and the supporting body-segment and may even have to construct the supported postures through forward or inverse kinematics. This paper presented a posturing framework that can automatically generate feasible supported postures from the task-description and the CAD model of the objects forming the DHM's environment. In this paper, two major challenges were addressed, namely, the problem of automatically selecting the support-surfaces for a given task and the problem of computing postures that take support on the selected surfaces. The key contributions of this work are the autonomy in selecting supports and the ability to generate feasible support-postures that simultaneously optimise the position of the support-contact as well as the reaction forces at the contact. Thus, with the description of the task and the geometry of the environment as input, the framework can generate multiple feasible supported postures. Therefore, the designer can quickly try out and evaluate alternate designs and perform more realistic simulations with significantly less effort.

REFERENCES

[1] American College of Sports Medicine; Franklin, B.; Whaley, M.; Howley, E.; Balady, G.: ACSM's Guidelines for Exercise Testing and Prescription. American College of Sports Medicine Series. Lippincott Williams & Wilkins, 2000. ISBN 9780683303551.

[2] Cappelletto, J.; Potvin, J.R.: Lower body bracing behaviours during externally supported tasks with extended reaches. International Journal of Human Factors Modelling and Simulation, 7(1), 1–12, 2019.

[3] Cappelletto, J.; Smets, M.; Liebregts, J.; Potvin, J.R.: A survey of leaning and bracing behaviours in an automotive assembly plant. International Journal of Industrial Ergonomics, 58, 33–37, 2017.

[4] Chiang, J.; Stephens, A.; Potvin, J.: Retooling jack's static strength prediction tool. Tech. rep., SAE Technical Paper, 2006.

[5] Ferguson, S.; Gaudes-MacLaren, L.; Marras, W.; Waters, T.; Davis, K.: Spinal loading when lifting from industrial storage bins. Ergonomics, 45(6), 399–414, 2002.

[6] Fewster, K.M.: AN INVESTIGATION OF LEANING BEHAVIOURS DURING ONE-HANDED SUBMAXIMAL EXERTIONS WITH EXTENDED REACHES. Ph.D. thesis, 2013.

[7] Garg, A.; Chaffin, D.B.: A biomechanical computerized simulation of human strength. AIIE Transactions, 7(1), 01–15, 1975.

[8] Holbein, M.; Redfern, M.: Functional stability limits while holding loads in various positions. International Journal of Industrial Ergonomics, 19(5), 387–395, 1997.

[9] Howard, B.; Yang, J.; Ozsoy, B.: Optimal posture and supporting hand force prediction for common automotive assembly one-handed tasks. Journal of Mechanisms and Robotics, 6(2), 021009, 2014.

[10] Howard, B.; Yang, J.J.; Yang, G.: Prediction of supporting hand forces for common automotive assembly tasks based on optimization and stability techniques for given posture. In ASME 2012 International Design Engineering Technical Conferences and Computers and Information in Engineering Conference, 641–650. American Society of Mechanical Engineers, 2012.

[11] Johnson, S.G.: The nlopt nonlinear-optimization package, 2014.

[12] Jones, M.L.; Kirshweng, R.L.; Armstrong, T.J.; Reed, M.P.: Force-exertion postures with external bracing in industrial tasks: data from an automotive assembly plant. In Proceedings of the Human Factors and Ergonomics Society Annual Meeting, vol. 52, 1049–1053. SAGE Publications Sage CA: Los Angeles, CA, 2008.

[13] Jones, M.L.; Reed, M.P.; Chaffin, D.B.: The effect of bracing availability on one-hand isometric force exertion capability. Ergonomics, 56(4), 667–681, 2013.

[14] Kingma, I.; van Dieën, J.H.: Lifting over an obstacle: effects of one-handed lifting and hand support on trunk kinematics and low back loading. Journal of Biomechanics, 37(2), 249–255, 2004.

[15] Kraft, D.: Algorithm 733: Tomp–fortran modules for optimal control calculations. ACM Transactions on Mathematical Software (TOMS), 20(3), 262–281, 1994.

[16] Liebregts, J.H.: An Investigation of External Support Choices and Behaviours During One-Handed Exertions with Constrained Reaches. Master's thesis, McMasters University, 2014.

[17] Pheasant, S.; Grieve, D.; Rubin, T.; Thompson, S.: Vector representations of human strength in whole body exertion. Applied Ergonomics, 13(2), 139–144, 1982.

[18] Plagenhoef, S.; Evans, F.G.; Abdelnour, T.: Anatomical data for analyzing human motion. Research quarterly for exercise and sport, 54(2), 169–178, 1983.

[19] Selvan, K.E.; Sen, D.: Estimating functional reach envelopes for standing postures using digital human model. Theoretical Issues in Ergonomics Science, 21(2), 153–182, 2020.

[20] Sunil, V.; Pande, S.: Automatic recognition of features from freeform surface cad models. Computer-Aided Design, 40(4), 502–517, 2008.